7-2024

Linkages of the 2022 Unprecedented Global Heatwave Events to Triple-Dip La Niña

Sachi Perera

Joshua B. Fisher

Mohamed Allali

Hesham el-Askary

Linkages of the 2022 Unprecedented Global Heatwave Events to Triple-Dip La Niña

LINKAGES OF THE 2022 UNPRECEDENTED GLOBAL HEATWAVE EVENTS TO TRIPLE-DIP LA NIÑA

Sachi Perera[1,4], Joshua B. Fisher[2], Mohamed Allali [2,3], Hesham El-Askary[2,4,5]

[1]Computational and Data Sciences Graduate Program, Schmid College of Science and Technology, Chapman University, Orange, CA 92866, USA
[2]Schmid College of Science and Technology, Chapman University, Orange, CA 92866, USA
[3]Fowler School of Engineering, Chapman University, Orange, CA 92866, USA
[4] Earth Systems Science and Data Solution Lab, Chapman University, Orange, CA 92866, USA
[5]Department of Environmental Sciences, Faculty of Science, Alexandria University, Moharem Bek, Alexandria 21522, Egypt

ABSTRACT

Heatwaves are influenced significantly by El Niño-Southern Oscillation (ENSO), which alters temperature and precipitation patterns throughout the world. Since 2020, we have witnessed a "triple dip" La Niña conditions persisting for three consecutive years resulting in severe weather and climate driven events globally. In this study, we identified the dominant frequency of Niño 3.4 Sea Surface Temperature (SST) signals and correlated them with regions experiencing unprecedented heat waves in 2022, namely, the Indian Ocean, the North Atlantic around England and Spain, and the Mediterranean Sea. The signal's power spectrum and its three highest power components are determined based on the signal's Singular Spectrum Analysis (SSA) for each region. Furthermore, the power spectrum coherence of Niño 3.4 and other study regions is obtained to determine whether ENSO and heatwaves are linked. We find that Niño 3.4 and the Indian Ocean have the same dominant frequency for the highest power received, indicating ENSO's influence on the Indian heat wave. Additionally, we discovered that in March 2022, the Jet stream is essential in bringing warm Arctic waves southward, passing through Niño 3.4 and India. Furthermore, we found that no other region shared the dominant frequency of the Niño 3.4 region.

1. INTRODUCTION

ENSO's impact on heatwaves varies geographically, highlighting the complex interplay between oceanic and atmospheric processes. El Niño is linked to elevated frequency, prolonged durations, and increased intensity of heatwaves, particularly in the southern regions [1]. A similar trend is evident in India, where El Niño results in more lengthy and intense heat waves due to a delayed Indian Summer Monsoon [2]. In Australia, the combination of ENSO and the Indian Ocean Dipole (IOD) can lead to more extensive and prolonged heatwaves, especially during strong El Niño events and occurrences coinciding with a robust positive IOD [3]. ENSO significantly influences heatwaves in Europe, impacting warm and cold extremes that affect mid-latitude circulation patterns in the North Atlantic/European sector [4]. The primary signal indicates colder conditions over Northern Europe during El Niño, accompanied by corresponding circulation anomalies [5]. These studies highlight the intricate and diverse impacts of ENSO on heatwaves, emphasizing the necessity for additional research to enhance our understanding and prediction of these phenomena globally.

2. DATA AND STUDY REGIONS

The Niño 3.4 region, located in the equatorial Pacific Ocean between 5°N and 5°S latitude and 120°W to 170°W longitude, plays a crucial role in observing and comprehending the El Niño-Southern Oscillation (ENSO). The SST in this area serves as a vital characteristic for ENSO events, shaping global climate patterns. During El Niño occurrences, the Niño 3.4 region encounters higher-than-usual SST, leading to disruptions in average atmospheric circulation and initiating various climate effects on a global scale. We use the "NOAA High-resolution Blended Analysis of Daily SST and Ice" datasets to collect ocean temperature data for 2022 (Figure 1). Study regions include those near India, England, and the Mediterranean, where heat waves were observed in 2022. The hot spot results are also compared with those of Niño 3.4, and near Spain (Figure 1).

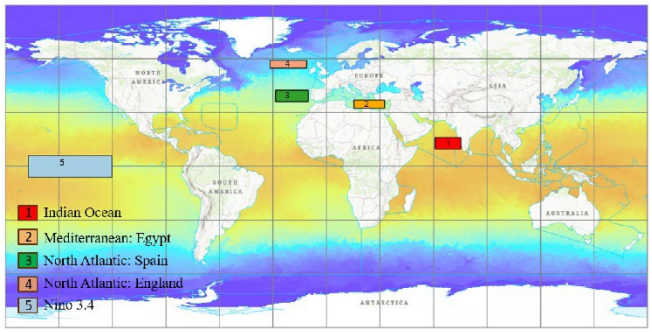

Figure 1: Regions experienced heat waves during 2022 and other study locations.

3. METHODS

3.1. Singular Spectrum Analysis (SSA)

Singular Spectrum Analysis (SSA) is a potent and versatile technique for analyzing time series to extract meaningful insights from complex and noisy data. The core principle of SSA involves breaking down a time series into its inherent components, thereby unveiling underlying patterns and trends. In SSA, the transformation of a time series into a trajectory matrix is followed by applying Singular Value Decomposition (SVD) to this matrix. The outcome of this decomposition is pairs of distinct values and singular vectors, serving as the principal components of the initial time series. These main components effectively capture the prevailing patterns and variations embedded in the data. The reconstructed components can subsequently be combined to restore the original time series or to decompose specific features like trends, seasonality, or noise (Vautard et al. 1992). SSA incorporates three fundamental steps (Vautard et al. 1992):

Step (i): The collected time series $\{X_n: n = 1, \ldots, N\}$ is transformed into a vector space with a dimension of M by including M lagged copies $\{X_{n-m}: m = 0, \ldots, M-1\}$. However, selecting the suitable value for M is not a straightforward task. [6] proposed that SSA is typically proficient in analyzing periods falling within the interval $(M/5, M)$.

Step (ii): The estimator for the M x M lag-covariance matrix, denoted as C_D, is established. Two commonly employed techniques are available for determining C_D. In the [7] algorithm, a window of length M moves through the time series, producing a sequence of $N' = N - M + 1$ vectors in the embedding space. This sequence is then used to construct the $N'\ x\ M$ trajectory matrix, X, where each row corresponds to a particular view of the time series within the window. In the [7] method, C_D is directly formulated through the matrix product.

$$C_D = (1/N')\, X^T X \qquad (1)$$

Step (iii): The covariance matrix, obtained from the N sample points using either the [7] or (Vautard and Ghil 1992) algorithm, is subjected to diagonalization. The resulting eigenvalues are then arranged in descending order. Each eigenvalue signifies the variance of the time series in the direction specified by its corresponding eigenvector. The square roots of these eigenvalues are termed singular values, collectively forming the singular spectrum. These terms collectively contribute to the terminology of the SSA. [7] illustrated this process by employing SVD on the trajectory matrix. In a parallel approach, (Vautard and Ghil 1992) named them empirical orthogonal functions (EOFs), drawing an analogy with the meteorological terminology used in Principal Component Analysis (PCA) when applied in the spatial domain. We utilized the summarized steps to compute the dominant frequency for the study regions mentioned above (Vautard and Ghil 1992).

3.2. Power Spectrum Coherence

Power Spectrum Coherence is a valuable metric in signal processing that assesses the degree of synchronization between two signals in the frequency domain. By combining concepts from Power Spectral Density (PSD) and coherence, Power Spectrum Coherence offers insights into the temporal relationships between different frequency components of signals. It calculates the coherence between the power spectral densities of two signals, quantifying how much the power in specific frequency components of one signal correlates with the power in the same frequency components of another signal.

4. RESULTS

4.1. Reconstructed Components (RC) for the Different Study Regions

Reconstructed components are obtained using the methodology described in 3.1 for the Niño 3.4 region (Figure 2) and the other four regions (Figure 3). As illustrated in Figure 2a, RC1 captures more variability in the Niño 3.4 signal than RC2 (Figure 2b). When RC1 and RC2 are combined, they jointly capture similar information found in the original signal. Furthermore, the complete reconstruction of the time series involves adding up these reconstructed components, ensuring no loss of information. In Figure 2c, the original time series is fully reconstructed by summing all reconstructed components, yet RC1 remains effective in capturing signal variations even with a reduced number of dimensions. Consequently, we proceeded with RC1 to calculate dominant frequency and coherent estimates, which exhibit the maximum proportion of variance of 73.52 with reduced dimensions compared to 19.04, the proportion of variance explained by RC2.

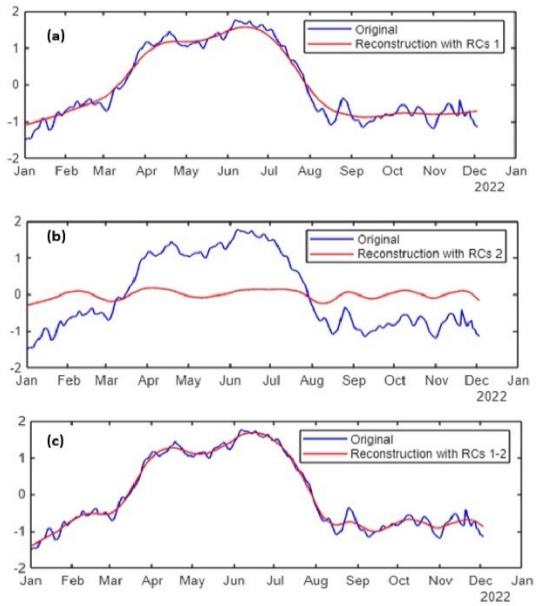

Figure 2. Comparison of reconstruction with first two components of Niño 3.4 signal

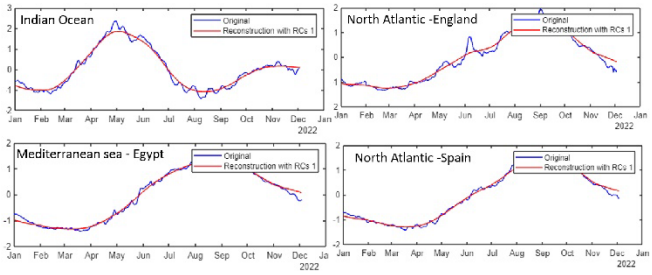

Figure 3. Comparison of reconstruction with first components of other regions

According to Figure 3, a similar approach was employed to examine SST signals in all other regions, resulting in the extraction of RC1 for each area that singularly encapsulates most of the information within the signal. Additionally, it is worth mentioning that the peaks of Niño 3.4 and Indian Ocean signals align during the Spring season. In the summer of 2022, the North Atlantic regions surrounding England and Spain and the Mediterranean Sea around Egypt experienced peak ocean temperatures. A peak in ocean temperatures was observed in the North Atlantic area surrounding England and Spain, as well as in the Mediterranean Sea area around Egypt, during summer 2022.

4.2. Power Spectrum Coherence of Niño 3.4 and study regions

The power spectrum of a signal, obtained through the Fourier transform, illustrates how its power is distributed across the frequency spectrum. Coherence, a statistical parameter ranging from 0 to 1, measures the linear association between two signals at different frequencies. A coherence value approaching 1 indicates a strong correlation, signifying that the signals either share information or are synchronized at that frequency. Conversely, a coherence nearing 0 suggests a lack of correlation or differing frequency characteristics between the signals.

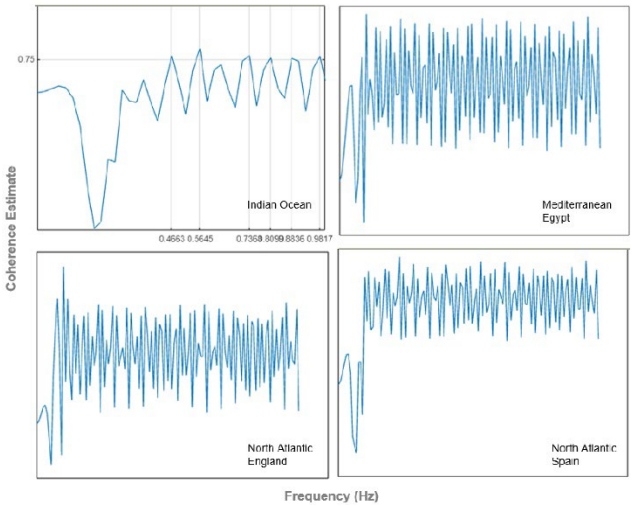

Figure 4. Power spectrum coherence of Niño 3.4 and study regions

Figure 4 shows that there are analogous dominant frequencies between Niño 3.4 and the Indian Ocean as compared to the other study regions that showed no apparent coherence. The coherence in the power spectrum between Niño 3.4 and the different areas examined in Figure 4 corresponds with the distinctive frequency components outlined in Table 1 for the North Atlantic and Mediterranean.

Table 1: Comparison of power and corresponding frequency obtained from the power spectrum.

	Niño 3.4	Indian Ocean	North Atlantic England	Mediter-ranean: Egypt	North Atlantic: Spain
Power Spectra	0.7804	0.6458	0.9015	0.9074	1.0064
	0.0416	0.0022	0.0405	0.0061	0.0101
	0.0072	0.0011	0.0024	0.0021	0.0023
Frequency	**0.0245**	**0.0245**	0.0123	0.0111	0.0123
	0.0614	0.0982	0.0491	0.0614	0.0491
	0.0982	0.1473	0.1104	0.0859	0.1104

Furthermore, using the power spectrum, the first three components with the highest power and corresponding frequencies are derived employing SSA decomposed signals (Table 1). Table 1 shows that Niño 3.4 and the Indian Ocean share the dominant frequency related to

the highest power obtained. This suggests potential evidence of ENSO impacting the Indian heatwave in 2022. Additionally, none of the other regions share the dominant frequency of the Niño 3.4 region. Table 1 reveals that the frequency values deviate compared to Figure 4, a difference that can be attributed to variations in the sampling frequency.

4.3. Shifts in Jet Streams during the 2022 Indian Heatwaves

Based on historical data, there is approximately a 60-75% probability that La Niña will lead to a stratospheric warming event during a polar outbreak. Since 2020, we have witnessed a triple occurrence of La Niña, contributing to extreme weather and climate events. A polar outbreak is characterized by the intrusion of frigid polar air masses into lower latitudes, often causing a sudden and significant temperature decrease. The jet stream's behavior, a high-altitude, fast-flowing air current, plays a crucial role in the development of polar outbreaks. Typically displaying a wavelike pattern, jet stream facilitates the southward extension of polar air when it forms distinct northward and southward dips.

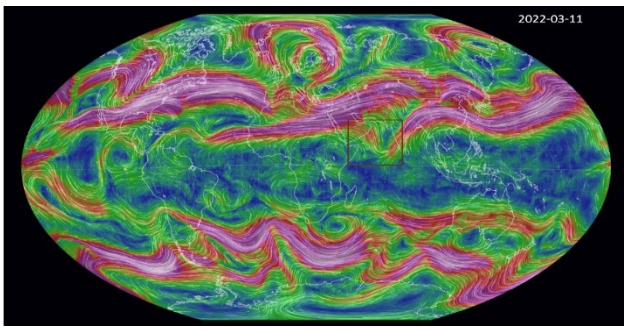

Figure 5: Shift of the jet streams during the Indian heatwave 2022

By utilizing the earth. null school [9] interactive app, we noted that in March 2022, the jet stream was vital in carrying warm Arctic waves southward toward the equator. It traversed through the Niño 3.4 region, giving rise to low-high pressure patterns in the vicinity of India.

5. CONCLUSIONS

El Niño occurrences are associated with increased surface temperatures and heatwaves, particularly in specific areas of India. Our findings indicate that Niño 3.4 and the Indian Ocean, where high low-pressure patterns were identified, consistently display a dominant frequency aligned with the highest power observed. This suggests a potential correlation between ENSO and the heatwave experienced in India in 2022. In contrast, other regions do not exhibit the dominant frequency observed in the Niño 3.4 region. This analysis proves that ENSO was crucial in influencing the specific heatwave patterns in the Indian region during 2022.

6. ACKNOWLEDGEMENT

The authors would like to acknowledge the support from the US Department of Education, award number P116Z230273, “Promoting the integration of Earth observations for Sustainable Development Goals”.

7. REFERENCES

[1] M. Luo and N.-C. Lau, “Amplifying effect of ENSO on heat waves in China,” *Clim Dyn*, vol. 52, no. 5, pp. 3277–3289, Mar. 2019, doi: 10.1007/s00382-018-4322-0.

[2] K. K. Murari, A. S. Sahana, E. Daly, and S. Ghosh, “The influence of the El Niño Southern Oscillation on heat waves in India,” *Meteorological Applications*, vol. 23, no. 4, pp. 705–713, 2016, doi: 10.1002/met.1594.

[3] P. J. Reddy, S. E. Perkins-Kirkpatrick, and J. J. Sharples, “Interactive influence of ENSO and IOD on contiguous heatwaves in Australia,” *Environ. Res. Lett.*, vol. 17, no. 1, p. 014004, Dec. 2021, doi: 10.1088/1748-9326/ac3e9a.

[4] K. Fraedrich, “An ENSO impact on Europe? - A review,” vol. 46, no. 4, Art. no. 4, Jan. 1994, doi: 10.3402/tellusa.v46i4.15643.

[5] A. A. Scaife, “Impact of ENSO on European Climate,” 2010.

[6] R. Vautard, P. Yiou, and M. Ghil, “Singular-spectrum analysis: A toolkit for short, noisy chaotic signals,” *Physica D: Nonlinear Phenomena*, vol. 58, no. 1, pp. 95–126, Sep. 1992, doi: 10.1016/0167-2789(92)90103-T.

[7] D. S. Broomhead and G. P. King, “Extracting qualitative dynamics from experimental data,” *Physica D: Nonlinear Phenomena*, vol. 20, no. 2, pp. 217–236, Jun. 1986, doi: 10.1016/0167-2789(86)90031-X.

[8] R. Vautard and M. Ghil, “Singular spectrum analysis in nonlinear dynamics, with applications to paleoclimatic time series,” *Physica D: Nonlinear Phenomena*, vol. 35, no. 3, pp. 395–424, May 1989, doi: 10.1016/0167-2789(89)90077-8.

[9] R. Cohen, “Beautiful Supercomputer Visualization Of Global Weather Conditions Updated Every 3 Hours,” Forbes. Accessed: Jan. 04, 2024. [Online]. Available: https://www.forbes.com/sites/reuvencohen/2013/12/18/beautiful-supercomputer-visualization-of-global-weather-conditions-updated-every-3-hours/